Differential state-dependence of low and high firing neurons in the hippocampus

Hiroyuki Miyawaki, PhD†, Kamran Diba, PhD*

Department of Psychology, University of Wisconsin-Milwaukee, 2441 E Hartford Ave, Milwaukee, WI 53211

† Present address: Department of Physiology, Graduate School of Medicine, Osaka City University, Asahimachi 1-4-3, Abeno-ku, Osaka, 545-8585, Japan

* Lead Contact: diba@uwm.edu; Tel: 414-229-5740; Fax: 414-229-5219.

This manuscript contains 4 figures, no tables, and 3 supplementary figures.

This work is supported by NIH R01MH109170 to K.D.

The authors disclose that there are no off-label or investigational use, no conflicts of interest, and no clinical trials.

Abstract (148 words)

Recent evidence suggests that low and high firing neurons display different plasticity and dynamics. Here, we rank-ordered rat hippocampal CA1 units by firing rate and implemented a shuffle-correction to account for regression-to-the-mean. We found that sleep/wake states and state transitions affected lower and higher-firing neurons differently. Firing-rate changes within non-REM sleep, REM sleep, and state transitions from non-REM to REM all favored higher-firing neurons, with either smaller increases or stronger decreases among lower-firing neurons. In contrast, transitions from REM to non-REM sleep resulted in higher firing among lower-firing neurons and vice versa. In sum, these patterns yielded a net decrease of firing rates across sleep, with the largest decrease occurring in lower-firing cells, and a net increase over waking, with median quantiles showing the largest firing increases. Our results suggest greater plasticity in lower firing neurons and show that non-REM sleep plays a uniquely normalizing role in sleep.

Keywords

Firing-rate homeostasis, REM sleep, non-REM sleep, balanced excitation/inhibition, regression to the mean

In Brief (46 words)

Miyawaki and Diba analyzed CA1 firing patterns beyond regression-to-the-mean and found that sleep activity is dominated by high-firing neurons, while lower-firing neurons demonstrate the biggest long-term changes, suggesting greater plasticity among these cells. The transition from REM to non-REM uniquely provides a rebalancing of circuit excitability.

eTOC Blurb.

- Sleep patterns are dominated by high-firing neurons.
- Low-firing neurons demonstrate greater plasticity across sleep and awake.
- REM to non-REM transitions rebalance network excitability.

Introduction

Neurons fire to communicate at rates that vary between neurons and across time. The dynamic range of a neuron's firing is determined by a combination of membrane geometry, distribution and types of ionic conductances, and efficacy of synaptic inputs (Koulakov et al., 2009; Lim et al., 2015; Nigam et al., 2016; Roxin et al., 2011; Stuart and Spruston, 2015; Yassin et al., 2010), and can quickly change, altering the neuron's encoding properties (Cheng and Frank, 2008; Lee et al., 2012). Modulations in each of these properties can potentially alter a neuron's gain function or "excitability". Recent evidence suggests that a neuron's firing rate is homeostatically regulated (Hengen et al., 2013; Miyawaki and Diba, 2016; Vyazovskiy et al., 2009), and that modifications in membranes and synapses can work to maintain the neuron's dynamic range (Marder and Goaillard, 2006; Turrigiano, 2011). Several studies from different labs indicate that these modifications are at least partially state-dependent; the emerging picture is that firing rates of neurons increase during waking (Hengen et al., 2016; Miyawaki and Diba, 2016; Vyazovskiy et al., 2009) and decrease during sleep (Grosmark et al., 2012; Miyawaki and Diba, 2016; Vyazovskiy et al., 2009), in a perpetual dance around a dynamic range.

Each waking and sleep state features different levels of neuromodulators, which contribute uniquely to the excitability of neuronal circuits, network firing patterns, and the plasticity of their synapses (Brown et al., 2012; Hobson and Pace-Schott, 2002). For example, REM is characterized by high acetylcholine and low noradrenaline, serotonin and histamine levels, while waking and non-REM respectively feature high and low levels of these neuromodulators (Brown et al., 2012; Hobson and Pace-Schott, 2002). Unique brainstem and thalamocortical networks are also active within each state, producing state-specific oscillatory firing patterns (Brown et al., 2012; Saper et al., 2010; Weber and Dan, 2016). The differing neuromodulatory and network

backgrounds lead to different mean firing rates in REM, non-REM, and waking (Miyawaki and Diba, 2016; Vyazovskiy et al., 2009), but averaging masks significant variations within each state (Grosmark et al., 2012; Miyawaki and Diba, 2016). We recently showed that sleep yields a net decrease in the firing rates of hippocampal neurons, likely through synaptic downscaling (Tononi and Cirelli, 2014) triggered by sharp-wave ripples and sleep spindles during non-REM sleep, and incorporated in REM sleep (Miyawaki and Diba, 2016). However, it is not clear how each of these brain states, from onset to offset, affect neurons at different excitability levels. In particular, low and high firing neurons are presumed to be affected differently by activity-driven homeostasis and bear differing levels of plasticity (Grosmark and Buzsaki, 2016; Hengen et al., 2013; Koulakov et al., 2009; Lim et al., 2015). Understanding such effects is further complicated by regression to the mean (RTM), for which the null hypothesis allows that firing rates of low-firing neurons should increase and those of high-firing neurons should decrease. In this report, we aim to investigate changes in firing rates of neurons within different stages of sleep and the effects of transitions between sleep stages, while carefully controlling for RTM.

Experimental Procedures

We analyzed data previously recorded from hippocampal CA1 region of four rats. Details of the experimental protocols, including animals, surgery, electrophysiological recoding, spike detection and clustering, and sleep detection can be found in ref (Miyawaki and Diba, 2016) and are summarized below. All experimental procedures were in accordance with the National Institutes of Health guidelines and approved by the University of Wisconsin-Milwaukee Institutional Animal Care and Use Committee.

Animals, surgery, and electrophysiological recoding Four male Long-Evans rats (250 – 350 g; Charles River Laboratories, Wilmington, MA) were implanted with 64-ch silicon probes in the

dorsal hippocampus (2.00 mm lateral and 3.36 mm posterior from the bregma) under isoflurane anesthesia. Three were also surgically implanted with two stainless steel wires (AS 636, Cooner wire, Chatsworth, CA) in the nuchal muscles to record electromyography (EMG). After at least 5 days of recovery from the surgery, we recorded local filed potentials (LFP) and unit activities continuously for 12 hours in light cycles (9 a.m. – 9 p.m.) and 9 hours in dark cycles (9 p.m. – 6 a.m.), in 19 total sessions. Animals were water-restricted, and ran on a linear track daily from 6 a.m. – 9 a.m. Spike detection and clustering were done, as previously described (Miyawaki and Diba, 2016), on each 9 – 12 hr session separately. Animals were kept in 12-hour light/dark cycles throughout the experiment.

Sleep detection Waking and sleep were segregated based on head speed of the rats and amplitudes of the EMG. In an animal that did not have EMG electrodes, we used volume-conducted EMG derived from the brain electrodes instead of nuchal EMG (Schomburg et al., 2014; Watson et al., 2016). High theta periods were detected based on the ratio of power in the 5 – 10 Hz band over 1 – 4 Hz and 10 – 14 Hz bands, using a MATLAB script developed by Anton Sirota (Sirota et al., 2008). High theta during sleep identified REM sleep (Robinson et al., 1977), and the remaining was non-REM. REM and non-REM epochs < 50 s were excluded from analyses.

Change index and deflection index Change index (*CI*) was defined as $(FR_2 - FR_1)/(FR_2 + FR_1)$, where FR_1 and FR_2 are firing rates of a neuron. Neuronal population was separated into quintiles based on FR_1 within each epoch, and mean *CI* across epochs was calculated for each quintile. Because neuronal firing rates are log-normally distributed, the difference in logarithm of firing rates, $\Delta log(FR)$, has been used elsewhere to assess firing rate change (Watson et al., 2016). Although *CI* and $\Delta log(FR)$ generally behave similarly (see supplemental information), $\Delta log(FR)$

becomes singular when either FR_1 or FR_2 approach or equal zero. Therefore, in our analysis we opted to use *CI*.

In each analysis, we generated 2000 shuffled surrogates by randomly flipping FR_1 and FR_2, and obtained shuffled mean and 95% confident intervals. The deflection index (*DI*) was defined as difference of *CI* from the surrogate mean.

Simulation of additive and multiplicative changes. Starting with $n = 5000$ "true firing rates" in period 1 (TFR_1) obtained from a log-normal distribution in CA1 pyramidal cells during non-REM sleep (0.536 ± 0.686 Hz, $n = 50846$) (Miyawaki and Diba, 2016; Mizuseki and Buzsaki, 2013), and true firing rate in period 2 (TFR_2) was determined based on:

For no change: $TFR_2 = TFR_1$

For multiplicative decrease: $TFR_2 = (1 - a) \times TFR_1$

For additive decrease: $TFR_2 = TFR_1 - b$.

For our example, we set $a = 0.090$ and $b = 0.052$, to match the mean ratio and difference between non-REM epochs in non-REM$_i$/REM/nonREM$_{i+1}$ triplets.

We also considered additive noise (SD_a) and multiplicative noise (SD_m) estimated from these triplets:

$$SD_a = \sqrt{2} \cdot RMS\left(\frac{FR_{i,j} - FR_{i+1,j}}{2}\right),$$

$$SD_m = \sqrt{2} \cdot RMS\left(\frac{FR_{i,j} - FR_{i+1,j}}{(FR_{i,j} + FR_{i+1,j})/2}\right),$$

where $FR_{i,j}$ is the firing rate of cell j in period i, and $RMS(\bullet)$ is root mean square across all cells in all triplets (n=15555). Our example (Figure 1) was generated by inducing additive or multiplicative noise as follows (n=1,2):

for additive noise: $FR_n = TFR_n + N_a$,

for multiplicative noise: $FR_n = TFR_n \times (1+N_m)$,

where N_a and N_m were zero-mean Gaussian distributed random values whose SDs, SD_a and SD_m, were determined above (SD_a = 0.171, SD_m = 0.592).

Results

We first set out to understand the relationship between variability and RTM in a population of neurons with log-normally distributed firing rates. We reasoned that variability might be either "additive noise", affecting all neurons by an equal amount, or else "multiplicative noise", proportional to each neuron's firing rate (also see Experimental Procedures). These scenarios are depicted for two snapshots from a population of neurons (n = 5000) where the only change comes from the noise term (Figure 1A). Naturally, additive noise has a larger relative effect on low-firing neurons. However, under both scenarios, lower-firing neurons show an apparent increased firing, while higher-firing neurons show an apparent decreased firing. This is RTM and can confound evaluations of true effects (e.g. from sleep). To control for this RTM, we instated a shuffling method in which we randomly flipped before/after indices and repeated the analysis multiple times to obtain a surrogate distribution. Under either (additive/multiplicative) noise scenario this surrogate data provided us with valuable "control" shuffle means and confidence intervals for each quintile. We defined the "deflection index (*DI*)" as the difference between the observed change index (*CI*) and the surrogate mean within each quintile. These *DI*s were not significantly different from zero when changes were due only to noise (Figure 1A).

We then examined *DI*s under two scenarios with a simulated effect in addition to noise: when firing rates were decreased across the population, either multiplicatively (Scenario 1), by an amount proportional to each cell's initial firing rate (Figure 1B), or additively (Scenario 2), by a

fixed amount for all cells (Figure 1C). Parameters for these effects were chose to simulate real data across non-REM sleep (see Experimental Procedures). In both scenarios, despite the incorporated decrease, lower-firing neurons appeared to increase firing, based on the *CI*s. However, under Scenario 1 the evaluated *DI*'s correctly depicted a uniform decrease across the population (Figure 1B). Meanwhile the additive decrease under Scenario 2 produced a larger relative effect on the *DI* in low-firing cells than in high-firing cells (Figure 1C), as expected. Thus, the shuffle-method produces *DI*s that can effectively describe and differentiate the two scenarios under either noise model, and control for RTM.

We next applied this method to hippocampal firing changes within non-REM and REM stages of sleep. During non-REM sleep, the average firing rates of (putative) pyramidal neurons increased ($CI = 0.058 \pm 0.002$, $p<10^{-300}$, Wilcoxon signed-rank test; Figure 2A). While the *CI* alone appears to show the largest increase in low-firing cells, and a decrease in the highest-firing quintile, when shuffle corrected, in fact all quintiles, as well as (putative) interneurons, showed a firing-rate increase (Figure 2A). While lower-firing cells appeared to show a smaller relative increase, firing increases were more uniform when we separated epochs depending on time-of-day and sleep-history (Figure S1 A-C). During REM sleep, we found an overall net decrease ($CI = -0.030 \pm 0.003$, $p= 5.4 \times 10^{-19}$, Wilcoxon signed-rank test; Figure 2B), including in interneurons. This decrease was apparently additive: lower-firing cells showed the largest relative firing decreases over the course of a REM sleep epoch. The magnitude and significance of this decrease was, however, dependent on time-of-day and subsequent sleep/wake state (Figure S1 D&E). These changes did not appear to reflect a change in the balance between excitation and inhibition within the course of either non-REM or REM states (Dehghani et al., 2016).

While firing rates of neurons change within each sleep stage, they also change between different stages. How a change in neuromodulatory background between sleep stages affects lower- and higher-firing neurons has not explicitly been tested. We therefore compared firing-rate quintiles across transitions from the last third of non-REM to the first third of the subsequent REM epochs, and from the last third of REM to the first third of the subsequent non-REM epochs. Non-REM to REM transitions were marked by an overall decrease (CI = -0.186 ± 0.003, $p < 10^{-300}$, Wilcoxon signed-rank test; Figure 2C), with decreased firing in lower-firing cells but increased firing in higher-firing cells. Interneuron firing also increased, potentially driving some of the differences (Niethard et al., 2016). In contrast, when REM transitioned to non-REM sleep, lower-firing quintiles showed increased firing while higher-firing quintiles and interneurons showed a firing decrease (Figure 2D). Interestingly, this transition was the only one we investigated that was not comparatively dominated by higher-firing neurons, but was instead marked by a renormalizing effect on firing rates across quintiles. Thus, non-REM sleep was unique in providing the initial background state for the most uniform firing among the population of cells, potentially because of lower effective inhibition.

These patterns were remarkably stable across early and late sleep in both light and dark cycles but there were also some variations according to time-of-day and preceding/following states (Figure S1). Quantiles in non-REM sleep following waking in early light-cycle sleep (9 a.m. – 3. p.m.) did not show the otherwise typical firing increases (Figure S1), likely because firing rates were saturated following awake track running (6 a.m. – 9 a.m.) (Miyawaki and Diba, 2016); these patterns resumed shortly thereafter following REM sleep. It may be worth noting that this first non-REM sleep following behavior (often called “post-sleep”) is in fact the most widely investigated epoch across the circadian cycle (Genzel et al., 2014; Rasch and Born, 2013),

though it is the most anomalous. Additionally, in non-REM epochs that transitioned to waking, firing rates in fact decreased during the light cycle (when rats sleep most), but increased in the dark cycle. For REM sleep preceding non-REM, decreased firing was also observed mainly in the early light cycle (9 a.m. – 3. p.m.), while in REM before waking, a large decrease was seen in the late dark cycle (1:30 a.m. – 6 a.m.).

In a recent study, we observed extended (~ 5s) periods of low-amplitude sleep, within non-REM, marked by substantially decreased power in the hippocampal local field potential and cortical EEG < 50 Hz (Miyawaki et al., 2016). We referred to these as LOW states. We also detected microarousals (MAs), with waking EMG levels, during non-REM sleep (Watson et al., 2016). MAs were recently reported to yield differential firing rate effects among low- and high-firing prefrontal cortical cells. We therefore examined how LOW and MA states affect hippocampal firing patterns. Comparing firing rates in non-REM from before (pre-) to after (post-) LOW states or MAs (Figure 3A & 3C), the *CI* indicated increased firing in low-firing cells and decreased firing in high-firing cells, as reported for prefrontal neurons before and after microarousals (Watson et al., 2016). However, when we corrected for RTM, the firing increase actually occurred in higher-firing neurons, and lower-firing neurons decreased firing. Similarly, when we investigated firing changes across consecutive LOW states or MAs (Figure 3B & 3D), low-firing and high-firing neurons respectively appeared to increase and decrease firing, but this pattern reversed in the *DI*, shuffle corrected for RTM. These observations highlight the importance of correcting for RTM and suggest that LOW states differentially affect firing in lower and higher-firing cells.

To summarize and compare the effects we have observed for REM and non-REM sleep along with waking and the net result across sleep, we plotted changes in quintiles (and for

interneurons) on the same scale (Figure 4). This fixed scale well demonstrates that the largest changes occurred between, rather than within states and, aside from the REM to non-REM sleep transition, most changes were anti-normalizing. It also illustrates the comparative effects of transitions between waking and sleep. Within waking, firing rates increased (CI = 0.111 ± 0.010, p=1.9 × 10^{-27}, Wilcoxon signed-rank test; Figure S2A) and preferentially in median-firing neurons (Miyawaki and Diba, 2016). Falling asleep was marked by an increase in firing rates in all quintiles (CI = 0.254 ± 0.004, p<10^{-300}, Wilcoxon signed-rank test; Figure S2B), but with the largest increase in the median quintile. On the other hand, waking up from either non-REM (Figure S2C) or REM sleep (Figure S2D) was marked by a relatively larger decrease in low-firing neurons, which were again the quintile most readily changed. To evaluate how net hippocampal firing changed across entire sequences of non-REM/REM sleep (bottom, Figure 4), we compared the first third of non-REM_i to the first third of the subsequent non-REM_{i+1} epoch (Figure S2E). Consistent with our previous report (Miyawaki and Diba, 2016), we found that, overall, firing decreased in all quintiles, but with a larger effect in lower than in higher-firing neurons. Likewise, across longer extended sequences of non-REM and REM sleep (> 30 min without interruption > 60 sec), firing rates of lower-firing cells decreased more (Figure S2F). Interneuron firing decreased as well, illustrating that this firing decrease was not due to a rebalance in excitation and inhibition. Somewhat surprisingly, we did not observe similar changes when comparing the first third of REM_i to the first third of the subsequent REM_{i+1} epoch (Figure S2G). This may be because of greater firing variability or saturated firing during REM sleep (Miyawaki and Diba, 2016) that masks changes. We also considered the possibility that each neuron has its own set point within the log-normal range of firing rates, and that sleep and waking move neurons relative to their individual set points (Hengen et al., 2013). For this

analysis, rather than investigating changes across firing rates, we calculated ratio of firing rate for each neuron relative to their session mean firing rates and determined quantiles by combining all epochs. Interestingly, these patterns (Figure S3) were highly similar to those seen in Figure 4 without individual normalization.

Discussion

In this work, we aimed to understand how low and high firing neurons are affected during and across REM and non-REM sleep and waking states, which is important for a better understanding of the function(s) of sleep states in mammals. We tested for RTM under two conditions. In the presence of multiplicative noise, lower-firing cells showed an apparent firing increase while higher-firing neurons showed a similar apparent decrease. When noise was additive, lower-firing cells showed a relatively larger effect. Some combination of additive and multiplicative variability is likely to be present in neuronal recordings. Overall, this analysis advocates caution in interpretation of increases and decreases that affect lower and higher firing neurons respectively. RTM alone describes a basic homeostatic effect. By measuring changes relative to a surrogate distribution obtained by random shuffles of the real data, we were able to measure effects beyond RTM, with significance determined by effect size and variability in the data. We found that, in general, sleep states and state transitions do not affect neurons uniformly, but that the changes depend on the relative excitability of cells, which likely reflect a combination of neuromodulation of membrane excitability (Graves et al., 2012; Nadim and Bucher, 2014) and sleep-dependent network dynamics involving excitatory and inhibitory synaptic inputs to neurons (Dehghani et al., 2016; Niethard et al., 2016; Steriade et al., 2001; Stringer et al., 2016; Timofeev et al., 2001).

Most of the states and transitions we investigated favored (increased or maintained) high-firing cells over low-firing ones. Remarkably, the transition from REM to non-REM was the only point at which we saw a simultaneous increase in lower-firing cells and a decrease in higher-firing ones, which served to partially renormalize firing across the population. Such an equitable effect was also present when we evaluated each neuron's firing relative to its own session mean. Thus, upon transition from REM to non-REM, cells firing below their mean rates increased firing while those firing above their means decreased. This observation indicates that the onset of non-REM sleep, relatively devoid of neuromodulation (particularly acetylcholine), provides the most equitable condition for neurons of varying excitability. Interestingly, upon this transition we also observed decreased firing in interneurons even while the average firing of pyramidal cells increased. This suggests that non-REM onset provides a release from active inhibition during REM that allows for a rebalancing of pyramidal cell excitability, which is consistent with the greater relative effect of muscarine on several classes of inhibitory cortical interneurons (Kuchibhotla et al., 2016). Furthermore, atropine, a muscarinic acetylcholine antagonist, also produces increased bursting in hippocampal CA1 pyramidal neurons of lower excitability ("regular spiking") but decreased bursting in higher excitability ("bursting") cells (Graves et al., 2012). Another intriguing explanation for these observations is that during most of sleep, except non-REM, there is competition between assemblies of neurons, with the winner determined by the assemblies starting with a higher-firing advantage. Such a mechanism may be implemented in a recurrently connected circuit endowed with inhibition (Lee et al., 1999; Rutishauser et al., 2011; Yuille and Geiger, 1995), such as region CA3, one synapse upstream from our CA1 recordings, whereas non-REM sleep provides a release from this active inhibition (see also Stringer et al., 2016). On the other hand, a third possibility is that cholinergic levels

during REM sleep favor entorhinal cortex drive of region CA1 (Mizuseki et al., 2011; Schomburg et al., 2014) while non-REM favors recurrently-generated activity internal to the hippocampus (Hasselmo, 2006); but why these would have differential effects on low and high firing cells would require further investigation.

Nevertheless, following non-REM onset, as a non-REM epoch develops, neuronal firing rates increase (Grosmark et al., 2012; Miyawaki and Diba, 2016) for all cells. The shuffle-corrected firing increases were significant across quantiles, though exact patterns also depended on time-of-day and preceding/following states, (Figure S1). Likewise, following REM onset, as REM epochs developed, shuffle-corrected firing rates decreased across the population, and with a lower decrease in higher-firing neurons. More dramatically, the non-REM to REM transition led to a firing increase in the higher-firing cells, but a decrease in lower-firing cells. These patterns are largely consistent with multiplicative changes in firing rates coupled with additive decreases. These decreases therefore affect all neurons by a similar amount, regardless of whether they are high or low firing cells, and they are manifest by a higher-relative decrease in lower-firing neurons.

The net effects of these transitions, from the beginning of one non-REM epoch to the beginning of the next one, or from the end of waking to its subsequent onset, were consistent with previous reports (Miyawaki and Diba, 2016; Watson et al., 2016): firing rates decreased in all quantile over sleep, but preferentially in lower-firing neurons. Whereas large state and state-transition effects are likely attributed to the combination of excitability effects discussed above, we and others have conjectured that that the slower firing rate decreases over sleep are produced by synaptic downscaling (Grosmark et al., 2012; Miyawaki and Diba, 2016; Tononi and Cirelli, 2014; Vyazovskiy et al., 2009). Network modeling also supports the notion of a strong link

between the strength a neuron's connectivity and its firing rate (Lim et al., 2015; Olcese et al., 2010). If this conjecture is correct, the greater relative decrease in lower-firing neurons may be indicative of an additive decrease, in which all synapses are downscaled by the same amount, which would have the effect of improving signal-to-noise in higher-firing cells (Tononi and Cirelli, 2014). Meanwhile, during waking a greater firing increase was seen in the median-firing neurons. The final result appears tantamount to greater downscaling in the synapses of lower-firing, and greater potentiation and learning in the synapses of median firing neurons. Higher-firing neurons appear to show the least plasticity, perhaps as a consequence of rigidity or saturated synapses (Grosmark and Buzsaki, 2016; Watson et al., 2016). These distinctions may also reflect differences in neuronal subtypes within the CA1 pyramidal layer (Danielson et al., 2016; Mizuseki et al., 2011) that exist throughout the cortex (Molyneaux et al., 2007).

Acknowledgements

We are grateful for helpful comments from Cleiton Lopes Aguiar.

Figure legends

Figure 1

Simulated noise and firing decreases affect low- and high firing cells differently. Log-normally distributed firing rates (n = 5000) were simulated (see Experimental Procedures) with additive noise ($Noise_{add}$, left columns) and multiplicative noise ($Noise_{mult,}$ right columns). Top panels show density plots of firing rate with identity (white lines). Black crosses indicate means of FR_1 and FR_2. Cells were separated into quintiles (different shades of aquamarine) based on FR_1. Change indices (*CI*, middle panels) and deflection indices (*DI*, bottom panels) were calculated for each quintile. Gray bands show 95% confidence intervals obtained from surrogate (shuffle) distributions. (A) Because of regression to the mean, with noise alone, low- and high-firing quintiles had positive and negative *CI*s, respectively. However, shuffle-corrected *DI*s were not significantly different from zero. (B) With a multiplicative decrease, *CI*s showed similar patterns to noise (A), but *DI*s demonstrated a uniform decrease across quintiles. (C) In contrast, an additive decrease had a greater relative effect on lower-firing cells. Error bars indicate SEM.

Figure 2

Firing rate changes within sleep states and upon transitions between sleep states. Density plot of firing rates (top panels) with identity lines (white) and means (black crosses). Change indices (*CI*, middle panel) and deflection indices (*DI*, bottom panels) are shown for each quintile along with 95% confidence intervals (gray bands), as well as for interneurons. (A) Within non-REM (50846 pyramidal cells and 5694 interneurons in 925 epochs), firing rates increased across quintiles (shades of blue), with a greater increase in higher-firing neurons, not apparent in *CI*s. (B) Within REM (24113 pyramidal cells and 2782 interneurons in 456 epochs), an apparent

additive decrease was observed, showing a greater decrease in low-firing quintiles (shades of purple). (C) Upon transition from non-REM to REM (21832 pyramidal cells and 2523 interneurons in 405 transitions), an anti-normalizing change was observed: lower-firing cells decreased firing but high-firing cells increased firing. (D) In contrast, a normalizing change was observed upon transition from REM to non-REM (17385 pyramidal cells and 1989 interneurons in 326 transitions). Error bars indicate SEM, *** $p < 0.001$.

Figure 3

Firing rate changes across LOW amplitude sleep and micro arousal within non-REM epochs. (A, B) Density plots of firing rates (top panels), change indices (*CI*, middle panels), and deflection indices (*DI*; bottom panels) were calculated between non-REM (NREM) periods before and after LOW amplitude sleep (A; 185983 pyramidal cells 31408 interneurons in 4725 sequences, shades of aquamarine quintiles) (Miyawaki et al., 2016). In (B), consecutive LOW states, separated by non-REM, are compared (B; 66665 pyramidal cells and 32640 interneurons in 5359 sequences). (C, D) The same analyses was performed for microarousals (MAs) which interrupted non-REM sleep, here inclusive of LOW (C, 44574 pyramidal cells and 15056 interneurons in 2538 sequences) and consecutive MAs separated by non-REM (D, 102333 pyramidal cells and 78802 interneurons in 3444 sequences). * $p < 0.05$, *** $p < 0.001$.

Figure 4

Firing rate changes across sleep. Summary plot of changing deflection indices through multiple non-REM (NREM) and REM epochs (see also Figure S2) shown on the same scale. Top panels depict average changes within epochs (note also Figure S1: these can vary depending on time-of-day and preceding/following states), and upon transitions. Bottom panels show changes from the first third of $NREM_i$ (or REM_i) to the first third of $NREM_{i+1}$ (or REM_{i+1}) for all

quintiles, as well as changes from the last minute of waking before sleep ($Wake_i$) to the first minute of waking after sleep ($Wake_{i+1}$). Error bars indicate SEM.

Supplemental Information

Change index and difference in log firing rate. Because neuronal firing rates are log-normally distributed, a recent study used the difference of log firing rates ($\Delta logFR$) to evaluate firing changes across sleep (Watson et al., 2016). We therefore compared this measure to the *CI* we use here and elsewhere (Miyawaki and Diba, 2016). When firing rates $FR_i = TFR \pm N$ (I = 1,2), (true firing rate plus noise) $\Delta LogFR$ and *CI* are given as follows:

$$\Delta logFR = \log(FR_2) - \log(FR_1) = \log\left(1 + \frac{2N}{TRF - N}\right),$$

$$CI = \frac{FR_2 - FR_1}{FR_2 + FR_1} = \frac{N}{TRF}$$

Thus, $\Delta logFR$ and *CI* are related by:

$$\Delta logFR = \log\left(1 + \frac{2CI}{1 - CI}\right)$$

When $N << TRF$, $\Delta logFR \sim CI$. However, when $N \rightarrow TFR$ (and/or $FR_i \rightarrow 0$), unlike *CI*, $\Delta logFR$ diverges. We therefore prefer to employ the *CI* to evaluate changes.

Supplemental Figure Legends

Figure S1

Changes within non-REM are affected by the timing and history of sleep. Deflection indices (*DI*) were calculated within non-REM epochs that followed waking (A), interleaved REM (B) or

preceded waking (C) in early light (9 a.m. – 3 p.m,; top row), late light (3 p.m. – 9 p.m.; second row), early dark (9 p.m. – 1:30 a.m.; third row) and late dark (1:30 a.m. – 6 a.m.; bottom row) periods, separately. In light cycles, firing rate did not further increase during non-REM following waking (A), likely because of saturated firing. Firing rate robustly and uniformly increased in non-REM interleaving REM (B). Unlike at other times, in non-REM preceding awake in light cycles (C), firing rates actually decreased. In REM preceding non-REM (D), firing decreases, affecting low-firing cells most strongly, were mainly seen in early light. In REM preceding waking (E), firing decreases were seen mainly in the late dark cycle. The number of analyzed cells are shown at top right corner in each plot (black for pyramidal cells, gray for interneurons). * $p<0.05$, ** $p<0.01$, *** $p<0.001$. Error bars indicate SEM.

Figure S2

Firing rate changes at state transitions. Density plots of firing rates (top) with identity lines (white) and means (cross), change indices (*CI*; middle) and deflection index (*DI*; bottom) in each quintile of pyramidal cells are shown, along with interneurons. Gray bands indicates surrogate mean and 95% confidence intervals. The comparisons are as follows: (A) first and last minutes of stable waking (1775 pyramidal cells and 54 interneurons in 46 stable wake), (B) state transitions from last minute of awake to first third of non-REM (NREM; 14494 pyramidal cells and 1508 interneurons in 251 transitions). (C) transitions from last third of non-REM to first minute of awake (12049 pyramidal cells and 1372 interneurons cells in 214 transitions), (D) transitions from last third of REM to first minute of awake (1802 pyramidal cells and 241 interneurons in 32 transitions), (E) between the first third of non-REM epochs in non-REM_i/REM/non-REM_{i+1} triplets (15555 pyramidal cells and 1778 interneurons in 288 triplets), (F) last and first one minutes of awake separated by sleep (3800 pyramidal cells and 704

interneurons in 99 sleep), (G) first third of REM epochs in REM_i/non-REM/REM_{i+1} triplets (8690 pyramidal cells and 1051 interneurons cells in 167 triplets).

Figure S3

Summary of changes in normalized firing rates. Firing rates were normalized by the ratio of each neuron's firing rate to its session mean, pooled across epochs, then separated into quintiles. The same shuffling method as before was used to generate surrogates. Patterns were remarkably similar to those for log-normal (non-normalized) firing rates (Figure 4). Error bars indicate SEM.

References

Brown, R.E., Basheer, R., McKenna, J.T., Strecker, R.E., and McCarley, R.W. (2012). Control of sleep and wakefulness. Physiol Rev *92*, 1087-1187.

Cheng, S., and Frank, L.M. (2008). New experiences enhance coordinated neural activity in the hippocampus. Neuron *57*, 303-313.

Danielson, N.B., Zaremba, J.D., Kaifosh, P., Bowler, J., Ladow, M., and Losonczy, A. (2016). Sublayer-Specific Coding Dynamics during Spatial Navigation and Learning in Hippocampal Area CA1. Neuron *91*, 652-665.

Dehghani, N., Peyrache, A., Telenczuk, B., Le Van Quyen, M., Halgren, E., Cash, S.S., Hatsopoulos, N.G., and Destexhe, A. (2016). Dynamic Balance of Excitation and Inhibition in Human and Monkey Neocortex. Sci Rep *6*, 23176.

Genzel, L., Kroes, M.C., Dresler, M., and Battaglia, F.P. (2014). Light sleep versus slow wave sleep in memory consolidation: a question of global versus local processes? Trends Neurosci *37*, 10-19.

Graves, A.R., Moore, S.J., Bloss, E.B., Mensh, B.D., Kath, W.L., and Spruston, N. (2012). Hippocampal pyramidal neurons comprise two distinct cell types that are countermodulated by metabotropic receptors. Neuron *76*, 776-789.

Grosmark, A.D., and Buzsaki, G. (2016). Diversity in neural firing dynamics supports both rigid and learned hippocampal sequences. Science *351*, 1440-1443.

Grosmark, A.D., Mizuseki, K., Pastalkova, E., Diba, K., and Buzsaki, G. (2012). REM sleep reorganizes hippocampal excitability. Neuron *75*, 1001-1007.

Hasselmo, M.E. (2006). The role of acetylcholine in learning and memory. Curr Opin Neurobiol *16*, 710-715.

Hengen, K.B., Lambo, M.E., Van Hooser, S.D., Katz, D.B., and Turrigiano, G.G. (2013). Firing rate homeostasis in visual cortex of freely behaving rodents. Neuron *80*, 335-342.

Hengen, K.B., Torrado Pacheco, A., McGregor, J.N., Van Hooser, S.D., and Turrigiano, G.G. (2016). Neuronal Firing Rate Homeostasis Is Inhibited by Sleep and Promoted by Wake. Cell *165*, 180-191.

Hobson, J.A., and Pace-Schott, E.F. (2002). The cognitive neuroscience of sleep: neuronal systems, consciousness and learning. Nat Rev Neurosci *3*, 679-693.

Koulakov, A.A., Hromadka, T., and Zador, A.M. (2009). Correlated connectivity and the distribution of firing rates in the neocortex. J Neurosci *29*, 3685-3694.

Kuchibhotla, K.V., Gill, J.V., Lindsay, G.W., Papadoyannis, E.S., Field, R.E., Sten, T.A., Miller, K.D., and Froemke, R.C. (2016). Parallel processing by cortical inhibition enables context-dependent behavior. Nat Neurosci.

Lee, D., Lin, B.J., and Lee, A.K. (2012). Hippocampal place fields emerge upon single-cell manipulation of excitability during behavior. Science *337*, 849-853.

Lee, D.K., Itti, L., Koch, C., and Braun, J. (1999). Attention activates winner-take-all competition among visual filters. Nat Neurosci *2*, 375-381.

Lim, S., McKee, J.L., Woloszyn, L., Amit, Y., Freedman, D.J., Sheinberg, D.L., and Brunel, N. (2015). Inferring learning rules from distributions of firing rates in cortical neurons. Nat Neurosci *18*, 1804-1810.

Marder, E., and Goaillard, J.M. (2006). Variability, compensation and homeostasis in neuron and network function. Nat Rev Neurosci *7*, 563-574.

Miyawaki, H., Billeh, Y.N., and Diba, K. (2016). Low activity microstates during sleep. bioRxiv http://dx.doi.org/10.1101/067892.

Miyawaki, H., and Diba, K. (2016). Regulation of Hippocampal Firing by Network Oscillations during Sleep. Curr Biol *26*, 893-902.

Mizuseki, K., and Buzsaki, G. (2013). Preconfigured, skewed distribution of firing rates in the hippocampus and entorhinal cortex. Cell Rep *4*, 1010-1021.

Mizuseki, K., Diba, K., Pastalkova, E., and Buzsaki, G. (2011). Hippocampal CA1 pyramidal cells form functionally distinct sublayers. Nat Neurosci *14*, 1174-1181.

Molyneaux, B.J., Arlotta, P., Menezes, J.R., and Macklis, J.D. (2007). Neuronal subtype specification in the cerebral cortex. Nat Rev Neurosci *8*, 427-437.

Nadim, F., and Bucher, D. (2014). Neuromodulation of neurons and synapses. Curr Opin Neurobiol *29*, 48-56.

Niethard, N., Hasegawa, M., Itokazu, T., Oyanedel, C.N., Born, J., and Sato, T.R. (2016). Sleep-Stage-Specific Regulation of Cortical Excitation and Inhibition. Curr Biol *26*, 2739-2749.

Nigam, S., Shimono, M., Ito, S., Yeh, F.C., Timme, N., Myroshnychenko, M., Lapish, C.C., Tosi, Z., Hottowy, P., Smith, W.C., *et al.* (2016). Rich-Club Organization in Effective Connectivity among Cortical Neurons. J Neurosci *36*, 670-684.

Olcese, U., Esser, S.K., and Tononi, G. (2010). Sleep and synaptic renormalization: a computational study. J Neurophysiol *104*, 3476-3493.

Rasch, B., and Born, J. (2013). About sleep's role in memory. Physiol Rev *93*, 681-766.

Robinson, T.E., Kramis, R.C., and Vanderwolf, C.H. (1977). Two types of cerebral activation during active sleep: relations to behavior. Brain Res *124*, 544-549.

Roxin, A., Brunel, N., Hansel, D., Mongillo, G., and van Vreeswijk, C. (2011). On the distribution of firing rates in networks of cortical neurons. J Neurosci *31*, 16217-16226.

Rutishauser, U., Douglas, R.J., and Slotine, J.J. (2011). Collective stability of networks of winner-take-all circuits. Neural Comput *23*, 735-773.

Saper, C.B., Fuller, P.M., Pedersen, N.P., Lu, J., and Scammell, T.E. (2010). Sleep state switching. Neuron *68*, 1023-1042.

Schomburg, E.W., Fernandez-Ruiz, A., Mizuseki, K., Berenyi, A., Anastassiou, C.A., Koch, C., and Buzsaki, G. (2014). Theta phase segregation of input-specific gamma patterns in entorhinal-hippocampal networks. Neuron *84*, 470-485.

Sirota, A., Montgomery, S., Fujisawa, S., Isomura, Y., Zugaro, M., and Buzsaki, G. (2008). Entrainment of neocortical neurons and gamma oscillations by the hippocampal theta rhythm. Neuron *60*, 683-697.

Steriade, M., Timofeev, I., and Grenier, F. (2001). Natural waking and sleep states: a view from inside neocortical neurons. J Neurophysiol *85*, 1969-1985.

Stringer, C., Pachitariu, M., Okun, M., Bartho, P., Harris, K., Latham, P., Sahani, M., and Lesica, N. (2016). Inhibitory control of shared variability in cortical networks. BioRxiv *oi: http://dx.doi.org/10.1101/041103*.

Stuart, G.J., and Spruston, N. (2015). Dendritic integration: 60 years of progress. Nat Neurosci *18*, 1713-1721.

Timofeev, I., Grenier, F., and Steriade, M. (2001). Disfacilitation and active inhibition in the neocortex during the natural sleep-wake cycle: an intracellular study. Proc Natl Acad Sci U S A *98*, 1924-1929.

Tononi, G., and Cirelli, C. (2014). Sleep and the price of plasticity: from synaptic and cellular homeostasis to memory consolidation and integration. Neuron *81*, 12-34.

Turrigiano, G. (2011). Too many cooks? Intrinsic and synaptic homeostatic mechanisms in cortical circuit refinement. Annu Rev Neurosci *34*, 89-103.

Vyazovskiy, V.V., Olcese, U., Lazimy, Y.M., Faraguna, U., Esser, S.K., Williams, J.C., Cirelli, C., and Tononi, G. (2009). Cortical firing and sleep homeostasis. Neuron *63*, 865-878.

Watson, B.O., Levenstein, D., Greene, J.P., Gelinas, J.N., and Buzsaki, G. (2016). Network Homeostasis and State Dynamics of Neocortical Sleep. Neuron *90*, 839-852.

Weber, F., and Dan, Y. (2016). Circuit-based interrogation of sleep control. Nature *538*, 51-59.

Yassin, L., Benedetti, B.L., Jouhanneau, J.S., Wen, J.A., Poulet, J.F., and Barth, A.L. (2010). An embedded subnetwork of highly active neurons in the neocortex. Neuron *68*, 1043-1050.

Yuille, A.L., and Geiger, D. (1995). Winner-take-all mechanisms. In Handbook of Brain Theory and Neural Networks, M.A. Arbib, ed. (Mit Press), pp. 1--1056.

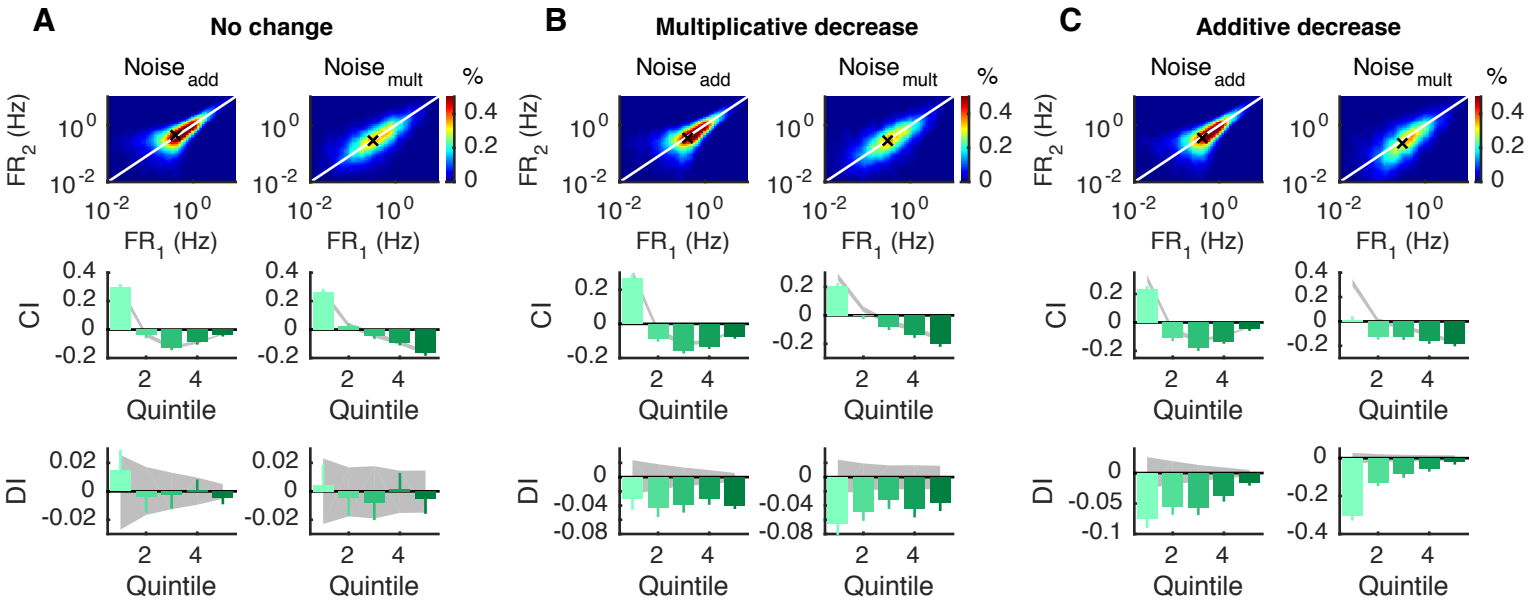

Figure 1

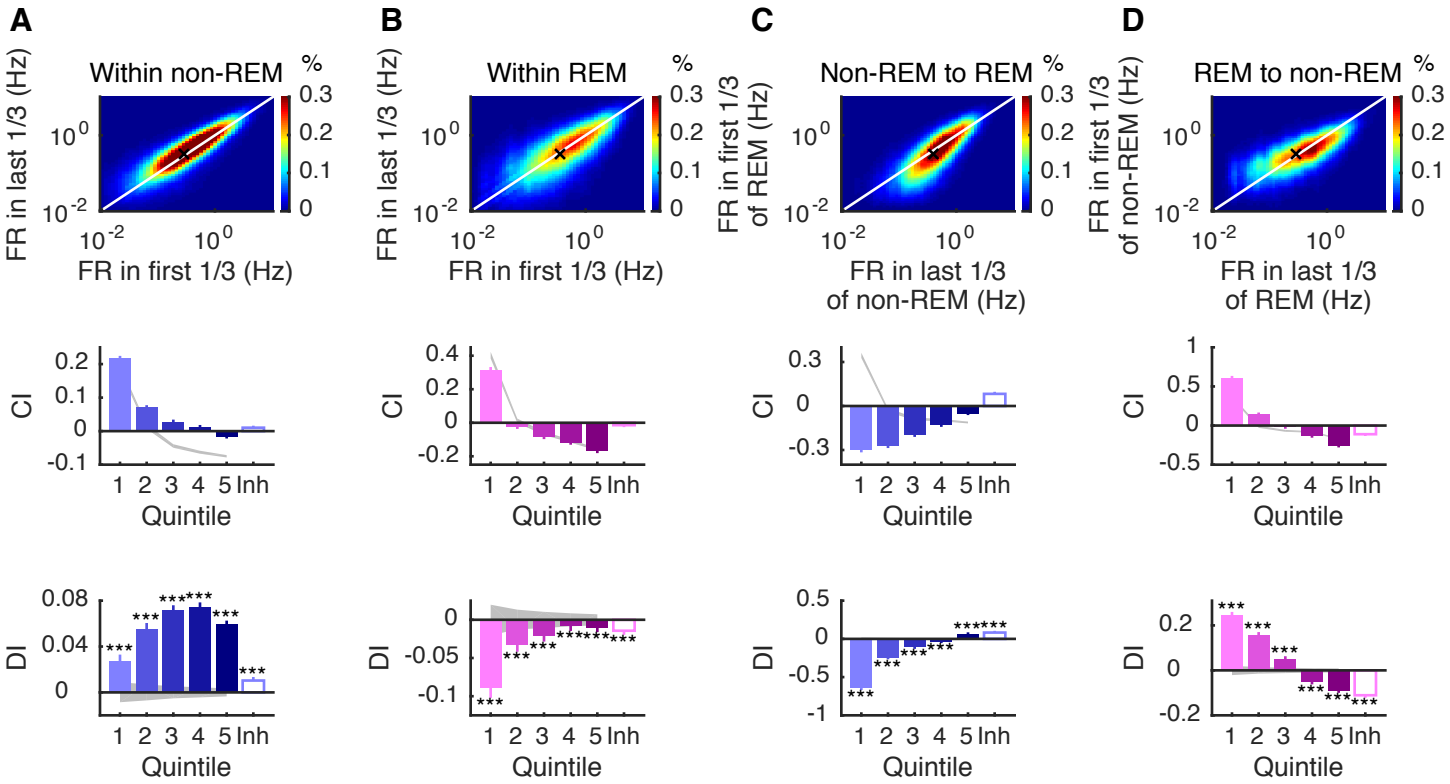

Figure 2

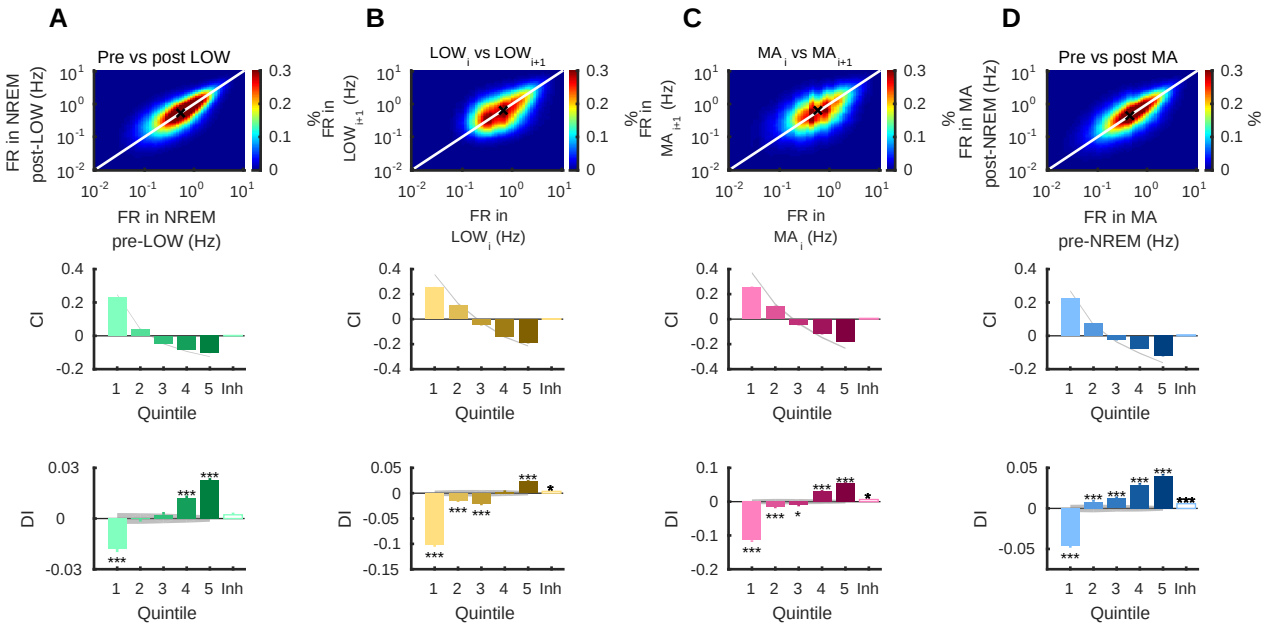

Figure 3

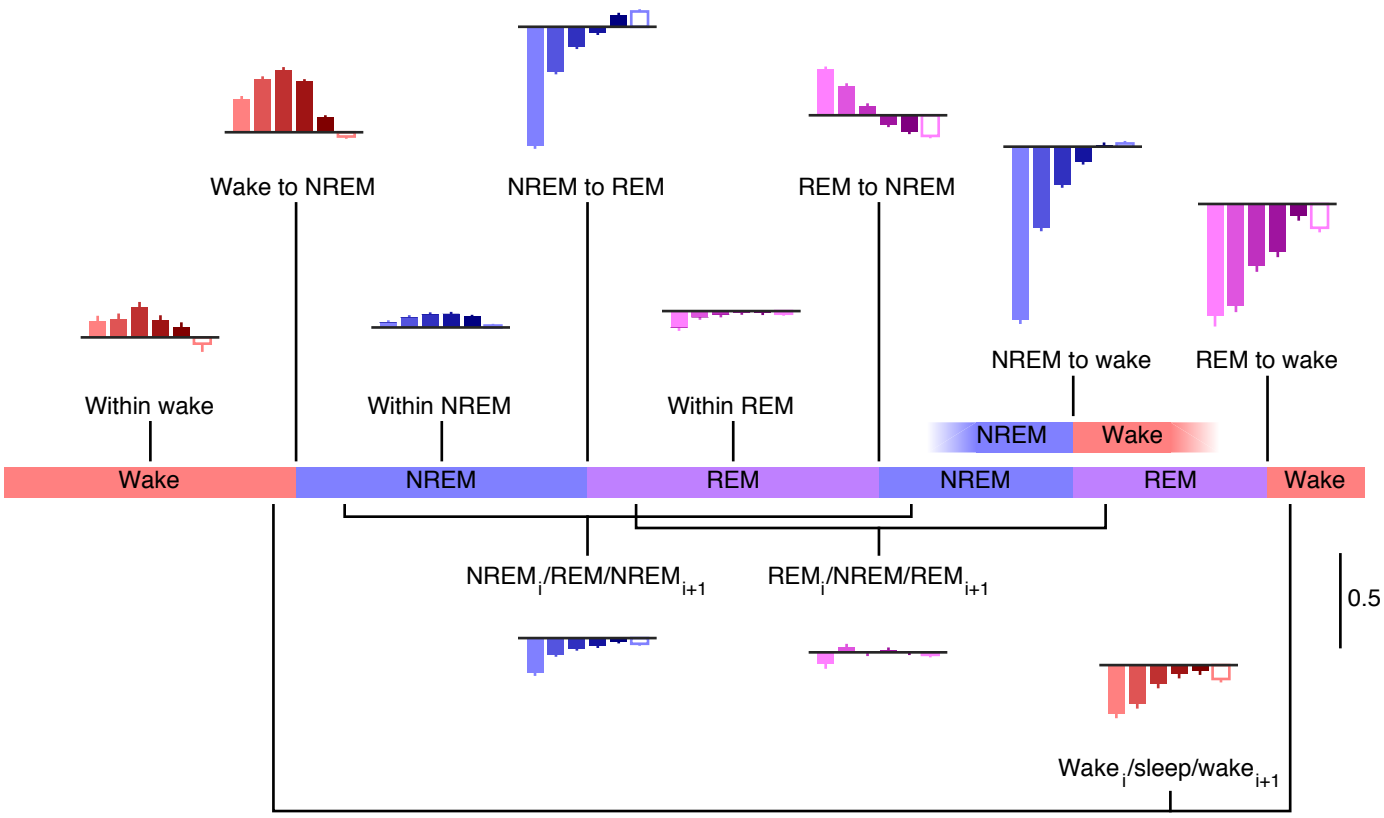

Figure 4

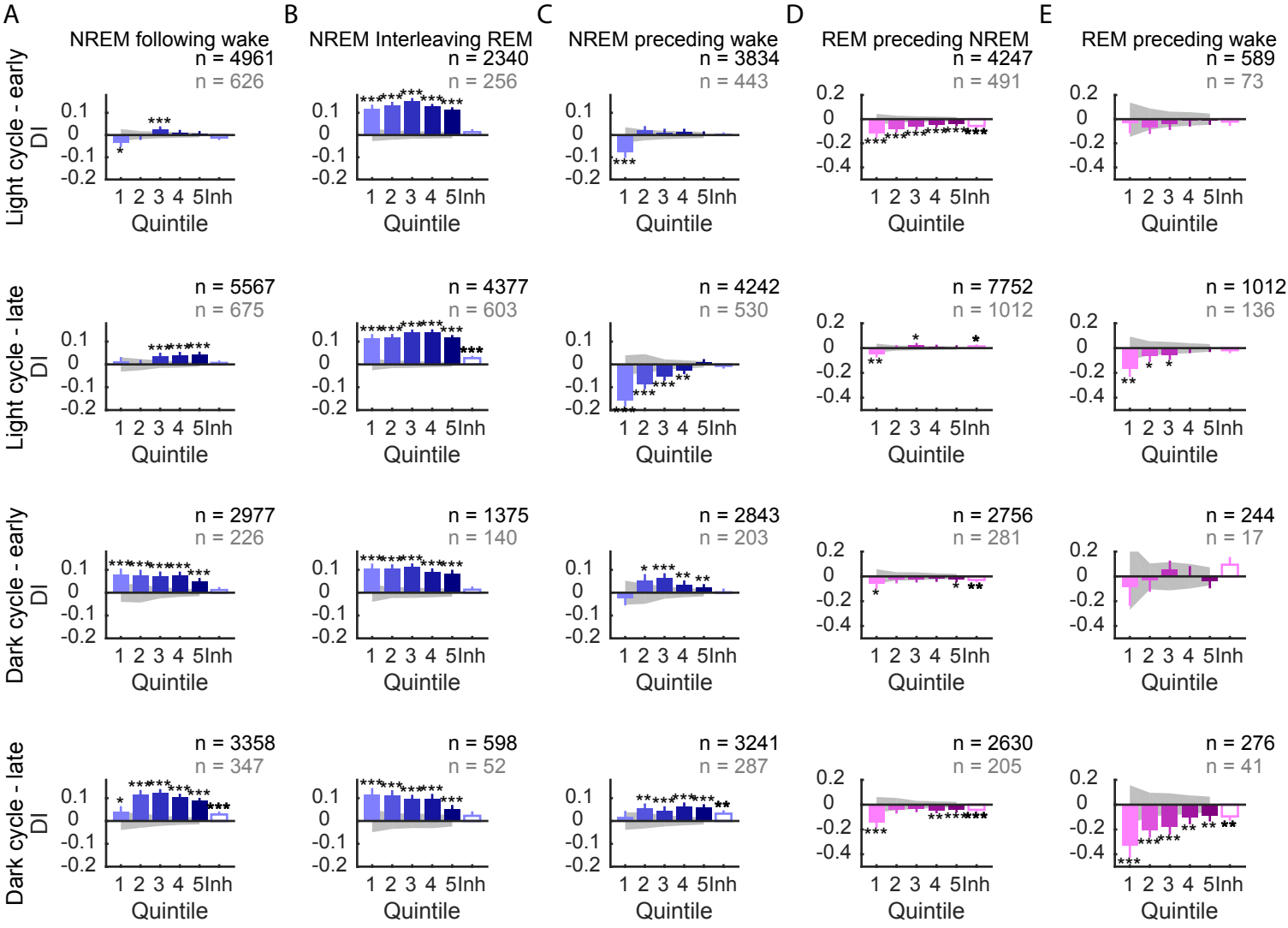

Figure S1

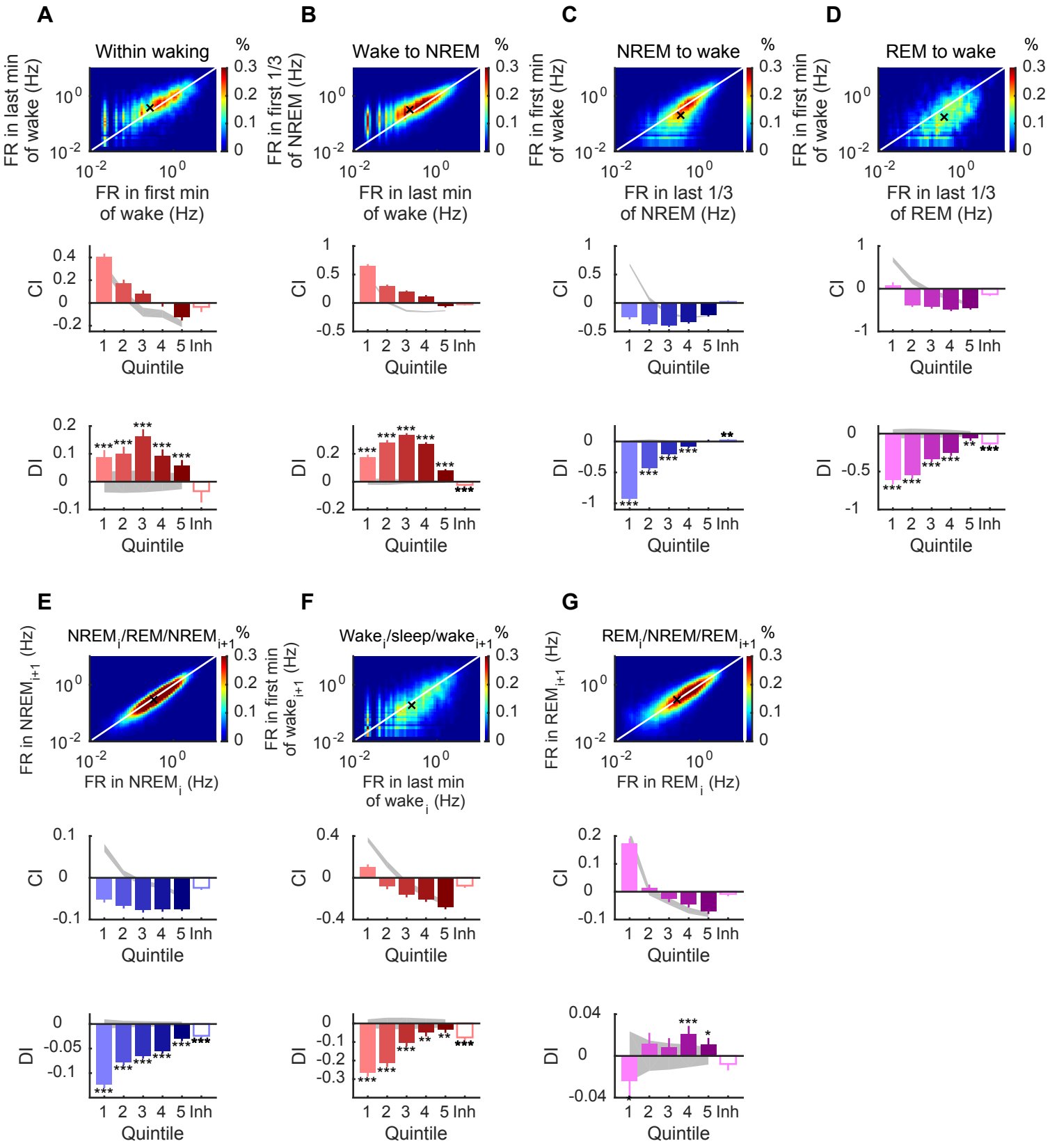

Figure S2

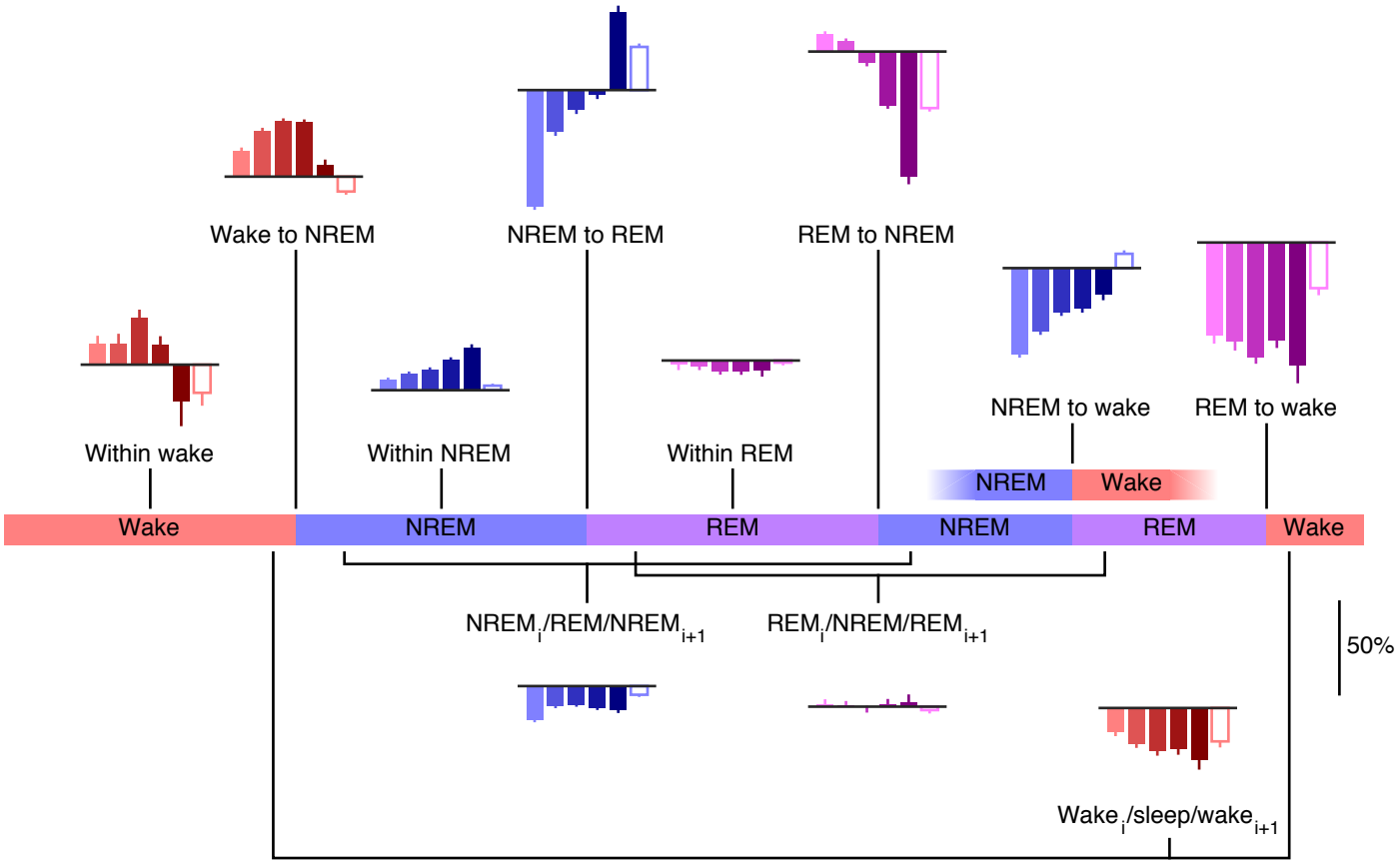

Figure S3